


Cite this: *RSC Adv.*, 2017, 7, 42363

High saturation magnetization superparamagnetic Fe/Ni core/shell microparticles for chromium removal

Zhaoqing Lu, Yanling Xu* and Shaomin Zhou *

In this paper, the Fe/Ni microparticles are synthesized by two reactions which directly utilize H₂ to reduce NiO and Fe₃O₄ microspheres. X-ray diffraction and transmission electron microscopy show that the as-synthesized Fe/Ni microparticles possess a body/face-centered cubic crystalline structure and core/shell morphology. The magnetic hysteresis loops show that the as-fabricated core/shell Fe/Ni microparticles have a high saturation magnetization (132.8 emu g⁻¹) at 305 K. The as-prepared Ni/Fe microparticles are used to remove Cr(vi) via a coupled adsorption/reduction process. The introduction of nickel not only controls the iron passivation but also advances efficient flow of electron transfer between iron and Cr(vi), thus efficient reduction of Cr(vi) to Cr(III). The excellent products with both high saturation magnetization and Cr(vi) adsorption capacity can be used as candidates for environmental remediation materials.

Received 11th April 2017
Accepted 10th August 2017

DOI: 10.1039/c7ra04104g

rsc.li/rsc-advances

1. Introduction

Chromium (Cr) is extensively used in electroplating, the leather and pigment industry and other fields, and it is one of the worst pollutants to the aquatic environment.^{1–3} Cr in the environment exists mainly in the form of Cr(III) and Cr(VI). Compared to Cr(III), the toxicity of Cr(VI) compounds toward human body is 100 times greater than that of Cr(III).⁴ Meanwhile, Cr(VI) with strong oxidation and migration abilities is also an important pollutant in water resources.⁵ Currently, there is a widespread concern over industrial waste water disposal containing Cr, and the most studied method of removing Cr(VI) is the chemical reduction method, in which Cr(VI) is reduced to Cr(III) with limited hydroxide solubility and much lower toxicity.⁶ Additionally, magnetic nanomaterials that can be controlled and moved under a magnetic field are promising reducing agents for Cr removal.

The application of magnetic nanomaterial could be broadened by shortening the time to separate it from the solution.⁷ A high saturation magnetization as an important parameter could facilitate rapid separation of the Cr from the wastewater by application of an external magnetic field.³ The bulk Fe is a kind of the magnetic material with high saturation magnetization whose saturation magnetization is up to 220 emu g⁻¹.^{8,9} Fe nanoparticle (NP) has high reaction and huge specific surface area,^{8,9} so it is usually used as an effective sorbent or reductant to degradation/removal some chemical pollutants.⁹ However, the saturation magnetization of Fe NP is relatively low, and Fe NP is very active

which is easily oxidized, so that the saturation magnetization is reduced hugely.^{8,9} Worse, the oxide layer would restrain the electron transfer, which decreases the effective use of Fe NPs.¹⁰ In order to protect and improve the reactivity of Fe NPs, adding the high saturation magnetization composition is a simple way where another magnetic metal should be chosen.¹¹ For example, Zhu *et al.*³ synthesize magnetic graphene nanocomposites with Fe cores which are used for rapid removal of Cr, and the saturation magnetization of nanocomposites is 96.3 emu g⁻¹. Unfortunately, such composite microparticle (MP) is incompatible with low expense of preparing procedure. In fact, as a catalytic metal, Ni is a magnetic material with low cost and good corrosion resistance, which is extensively utilized in wastewater treatment.¹² Firstly, the Ni and Fe can be used as primary cell, which can change the electronic properties of Fe. Among them, Ni acts as the electron transfer medium which would promote the series of reactions.¹⁰ In addition, the catalytic metal Ni has strong adsorption capacity for hydrogen molecules, which can enhance the formation of atomic hydrogen or hydride on the surface of the MPs.⁴

In our previous report,⁵ the as-synthesis Fe₃O₄/polypyrrole nanospheres possess good adsorption properties (209 mg g⁻¹) compared to other adsorbent materials, but the samples have low saturation magnetization (25.06 emu g⁻¹), which is difficult to quickly separate from the wastewater under the action of external magnetic field. In order to improve the saturation magnetization of composite, Fe/Ni MP is a good choice. Currently, the modified liquid-phase chemical reduction method^{4,10} has been used to prepare Fe/Ni composite, but the samples prepared by this method are prone to agglomeration, which limit application development. Because the samples prepared by the chemical vapor deposition (CVD) method have

Key Lab for Special Functional Materials of Ministry of Education, Henan University, Kaifeng 475004, People's Republic of China. E-mail: smzhou@henu.edu.cn; Fax: +86 371 23881358; Tel: +86 371 23885579



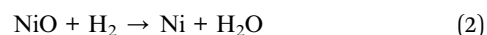
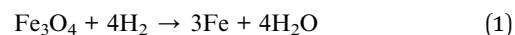
high crystallinity and fewer defects,¹³ here we report a CVD method for the synthesis of core/shell Fe/Ni MPs. We use NiO and Fe₃O₄ particles (based on our earlier work)^{5,6,8} as precursors, and the Fe₃O₄ particles are prepared through a solvothermal reaction. For the two reactions, firstly, Fe₃O₄ particles are reduced to Fe NPs by H₂, and secondly, NiO particles are reduced to Ni NPs by H₂. The magnetic hysteresis loops show that the samples exhibit superparamagnetism at 305 K. Furthermore, the saturation magnetization of the MPs can reach 132.8 emu g⁻¹, which is higher than the other ferro-matrix composites reported earlier.^{5,6,14,15} In particular, we also study the adsorption of Cr(vi) where Fe/Ni MPs on the Cr(vi) have a good adsorption effect.

2. Experimental details

The synthesis of samples was carried out in the oxygen-free condition of the quartz tube and the quartz tube was installed in the tube furnace. In this experiment, the pure NiO which was loaded in the crucible was placed in the upstream end, and the Fe₃O₄ microspheres precursors (0.35 g)⁵ were placed in the central high temperature region of the quartz tube. Prior to heating, the system with high purity Ar gas was flushed 1 hour in order to eliminate O₂ and then filled with enough pure H₂. Tube pressure and gas flow rate were maintained at about 60 Pa and about 15 standard cubic centimetres per minute (scm), respectively. The system was then in the central region of the furnace heated to 1400 °C, and maintained at this temperature for 5 h.

Then, turned off the hydrogen while the argon gas was fed at a flow rate of about 30 scm into the reactor to maintain an inert atmosphere, then the system was then in the central region of the furnace cooled to 1200 °C, and annealed at this temperature for 6 h. After completed, the samples with furnace cooling were collected after the furnace was cooled to room temperature.

The reaction of this process is given in two reactions following chemical equation:



The samples were extensively characterized for morphology, phase and chemical composition using scanning electron microscopy (SEM) (XL 30 S-FEG; Holland), X-ray powder diffraction (XRD) (X'pert MRD-Philips; Holland), transmission electron microscopy (TEM), high-resolution TEM (HRTEM), the energy dispersive X-ray spectroscopy (EDX), and high-resolution X-ray photoelectron spectroscopy (HRXPS). Magnetic properties were carried out using Quantum Design Superconductor Quantum Interference Device (SQUID) (MPMS XL7).

3. Results and discussion

3.1. Composition, structure and morphology of Fe/Ni core/shell MPs

Fig. 1a is a typical SEM of Fe/Ni MPs, high-density spherical nanostructures are observed, and the diameter of the MP is

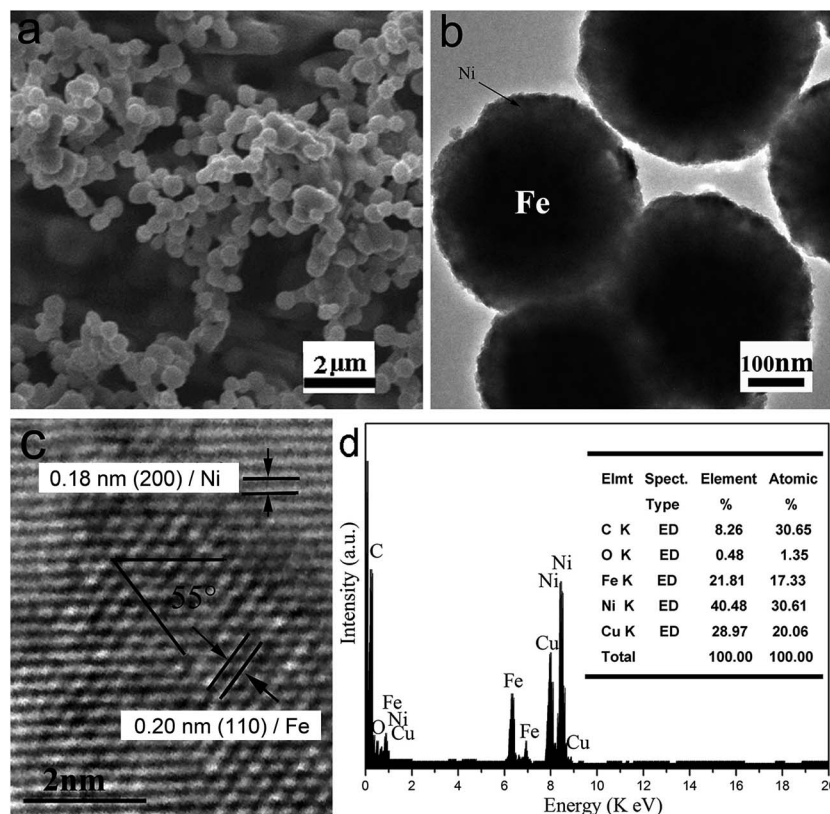


Fig. 1 Typical SEM (a), TEM (b), HRTEM (c) image and EDX pattern (d) of core/shell Fe/Ni MPs.



approx 400 nm. Fig. 1b is a typical TEM image of core/shell Fe/Ni MPs, it shows that the as-synthesized products are uniform and controlled diameter approx 400 nm. From the TEM image, we can observe the dark center region and the pale edge region of MP where periphery has a layer of 100 nm shell and 300 nm in the center. Through SEM and TEM images, we can further confirm that the synthesized samples are uniform MPs with core-shell structure. It can be seen from Fig. 1c that interplanar spacing at the edge of the MP is 0.18 nm, which corresponds to the lattice spacing of Ni (200) plane. The interplanar spacing at the center of the MP is 0.20 nm, which is found to be equal to that of Fe (110) plane through comparison. Based on micro-composition-analysis, Fig. 1d is the EDX spectrum, which shows only the Fe peak and Ni peak, and the Cu peak and C peak are attributable to the copper grid with carbon film.

To further determine the distribution of Fe and Ni, the TEM-EDX mapping is employed to characterize a Ni/Fe core/shell MP (Fig. 2a–c). As shown in Fig. 2a and c, it is sure that Ni compositions were evenly coated on the outside of the Fe core.

Fig. 3 shows the XRD pattern of the as-fabricated Fe/Ni MPs. The corresponding XRD diffraction peaks can be indexed to (110), (111), (200) and (222) planes. The diffraction peaks can be assigned to the Ni (fcc)/Fe (bcc) structure (JCPDS no. 040850/060696)^{8,16} and diffraction peaks are sharp. No impurity phase such as oxides or precursors is detected, so the purity of product is high, and it indicates a stoichiometric composition and phase of core/shell Fe/Ni MPs.

XPS is supposed to be a sensitive and powerful instrument to investigate the surface chemical composition/valence state of materials. In order to figure out the main mechanisms of Cr(vi) removal by Ni/Fe core/shell MPs and the change in the valence states of chemical elements, HRXPS is carried out to study the surface chemical compositions and valence of the materials obtained before and after their treating with chromium solution and the results are presented in Fig. 4. Fig. 4a shows the HRXPS of the Fe/Ni MPs before treating with chromium solution. The peaks located at 852.42 and 869.65 eV correspond to the binding energies of Ni 2p_{3/2} and Ni 2p_{1/2}, which indicates elemental Ni instead of compound Ni.^{4,10} These results further verify that the core/shell MP is composed of Ni and Fe. Because HRXPS is a truly surface analysis technique with only 2–5 nm probing depth, as core, iron is not

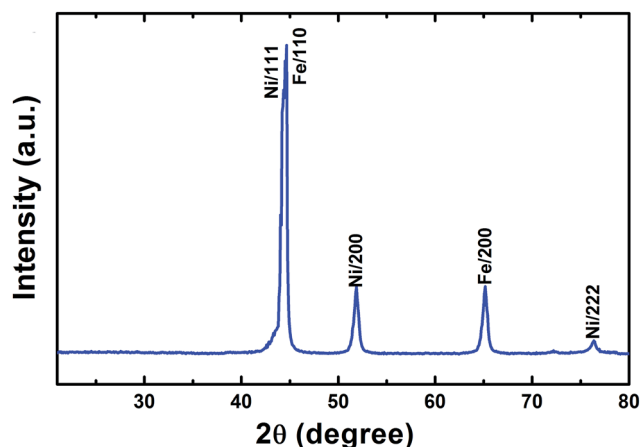


Fig. 3 Typical XRD patterns of the products.

detected in HRXPS. The XRD and XPS techniques prove that Fe⁰ exist only inside, which supports the existence of the core-shell structure of the Fe/Ni MPs. Fig. 4b gives the HRXPS of the valence of sample after treating with chromium solution, the binding energy of 852.7 eV, 855.3 eV and 869.8 eV are corresponding to Ni⁰ and Ni²⁺ 2p in the Fe/Ni composite. It is found that the peak of Ni⁰ appears weak after the treating with chromium solution, which indicates that single Ni⁰ is involved in redox (Ni²⁺) besides catalysis.⁴ Like earlier report, similar situations occur in other studies.¹⁷ Detailed HRXPS spectrum of the regions for Cr 2p is showed in Fig. 4c. The peaks for Cr 2p_{3/2} and 2p_{1/2} center at 576.6 and 585.9 eV respectively, indicating that Cr(III) is the predominant chromium species on the surface.¹⁸ This data further demonstrate that part of adsorbed Cr(vi) anions is reduced to Cr(III). The Cr 2p_{3/2} peak at 576.6 eV represents the formation of Cr(III) on the surface of Ni/Fe MPs. The Cr 2p_{1/2} peak at 585.9 eV represents Cr(III).¹⁹ However, there is no obvious band of Cr(vi) in the HRXPS spectrum of Ni/Fe MPs after contact with Cr(vi) solution, which is consistent with the previous study.²⁰ Cr(vi) removal process may involve the reduction of Cr(vi) into Cr(III), and consequent either adsorption or co-precipitation of reduction products, such as Cr(OH)₃, Cr₂O₃ and co-precipitation of Cr_xFe_{1-x}(OH)₃.¹⁰

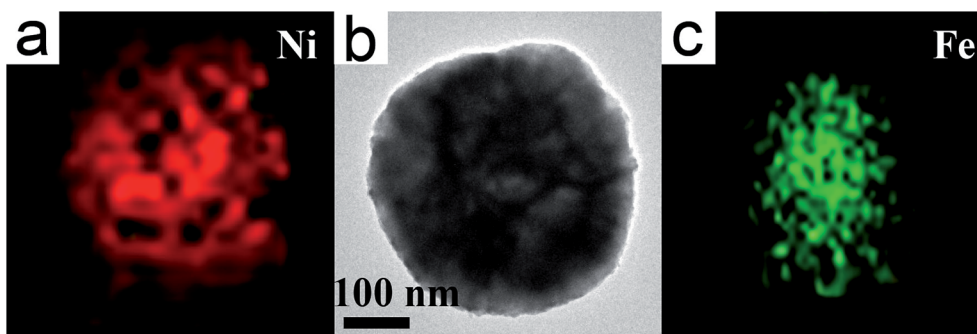


Fig. 2 The EDX Ni (a) mapping, TEM (b) image, and Fe (c) mapping of a single Ni/Fe core/shell MP.



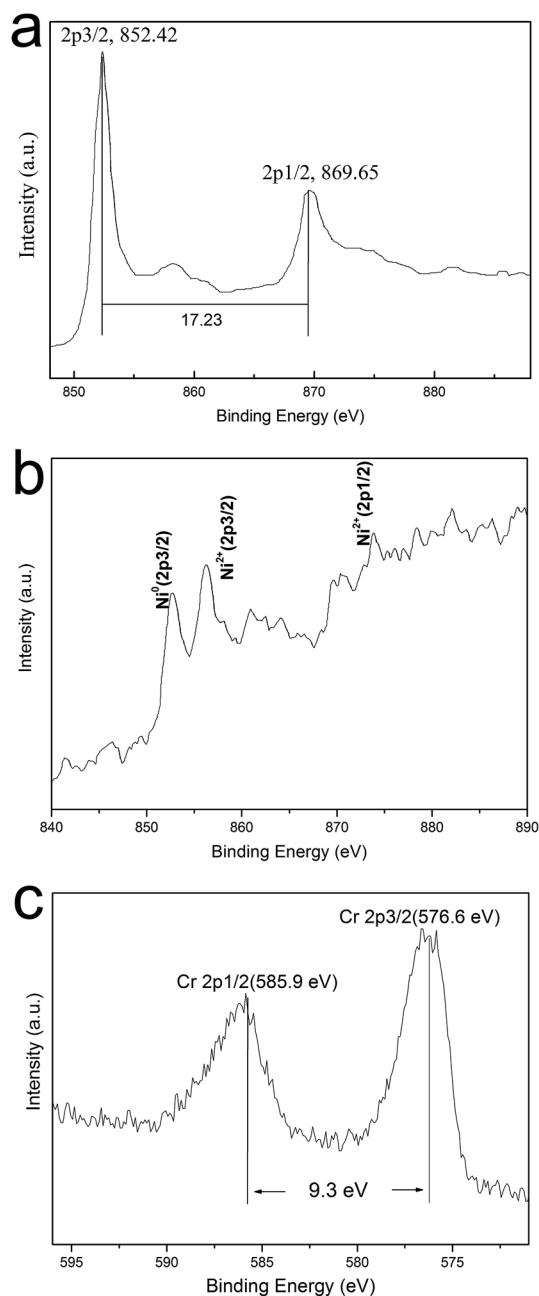


Fig. 4 HRXPS spectra of Ni 2p (a) before treating with chromium solution, Cr 2p (b) and Ni 2p (c) of Ni/Fe core/shell MPs after treating with chromium solution.

3.2. Growth mechanism

According to our experimental process as shown in Fig. 5, the mechanism of our two reactions growth of Fe/Ni core/shell MPs should be as follows. Firstly, in its infancy of reaction, Fe_3O_4 particles are reduced to a great quantity of primary Fe NPs by H_2 . However, the primary Fe NPs are very unstable in virtue of high surface energy, which results in the aggregation until it attains the lowest energy state.¹³ So, the scattered MPs with ~ 300 nm in size are distinctly obtained as an intermediate material Fe core at the initial reaction process. To examine the Ni shell growth process, the time evolution of Fe/Ni core/shell

MP is examined by observing TEM images of products obtained after 2, 3, 4, and 5 h of 1400°C (Fig. 5). The growth of Ni shell over Fe core starts from nucleation on only one selective side facet, where a semi-spherical nucleus is formed initially after 2 h (Fig. 5a). Subsequently, the more nuclei are formed and covered other facets of Fe core after 3–4 h (Fig. 5b and c). After 5 h, Ni shell is grown over fully Fe core, forming a typical core-shell structure (Fig. 5d).

3.3. The magnetic properties of specimens

Magnetic measurements are performed using a SQUID magnetometer in order to investigate the magnetic characteristics of the composite. Fig. 6a and b show the magnetization *versus* curves at 250 K and 305 K in a lower magnetic field (250 Oe). At lower temperature (250 K), the obtained MPs exhibit ferromagnetic behavior with saturation magnetization/ $M_s = 157 \text{ emu g}^{-1}$, coercivity/ $H_c = 12 \text{ Oe}$, and remanence/ $M_r = 7.2 \text{ emu g}^{-1}$. At higher temperature, however, the 305 K M (H) curve reflects superparamagnetic behavior of the MPs with a saturation magnetization $M_s = 132.8 \text{ emu g}^{-1}$, as well as zero for H_c and M_r . In order to increase the reliability of the experimental data, as shown in Fig. 6c and d, we test the magnetization at 10 K and 310 K in a higher magnetic field range from -5000 to $+5000$ Oe. Like the lower magnetic field mentioned above, the MPs at a lower temperature (10 K) also exhibit ferromagnetic behavior with $M_s = 157.4 \text{ emu g}^{-1}$, $H_c = 29.6 \text{ Oe}$, and $M_r = 7.1 \text{ emu g}^{-1}$ whereas the 310 K M (H) curve still reflects superparamagnetic behavior of the MPs with a $M_s = 132.9 \text{ emu g}^{-1}$ without coercivity and remanence. These features will provide an easy and efficient avenue for separating Fe/Ni composite particles from a suspension system under different external magnetic fields.

The temperature dependent magnetization (M - T) measurements for all the particles are carried out in the range between 2 and 350 K at 150 Oe field under zero-field-cooled (ZFC) and field cooled (FC) conditions. The data is presented in Fig. 7 and the obtained results confirm the freezing of the superparamagnetic fluctuation at blocking temperature $T_B = 300.3 \text{ K}$ indicates by a round maximum followed by a paramagnetic-like behavior at higher temperatures. At low temperature, the FC curve is flat, and the temperature difference between the maximum magnetization temperature and the blocking temperature supports the hypothesis.²¹ So above and below the blocking temperature ($T_B = 300.3 \text{ K}$), the core/shell Fe/Ni MPs are respectively shown superparamagnetic and ferromagnetic, which is consistent with the results of the magnetization *versus* curves.

For samples showing the high saturation magnetization ($M_s = 132.8 \text{ emu g}^{-1}$), we carry out the following analysis. Firstly, the samples prepared by CVD method have high crystallinity and fewer defects, so the spin magnetic moment chaos can be reduced, which makes the saturation magnetization improved.¹³ Secondly, although the M_s of single-crystalline bulk Fe at room temperature is up to 220 emu g^{-1} ,^{8,22} the M_s value of conventional Fe NPs should be somewhat smaller than that of counterpart bulk material. Unlike conventional Fe NPs,



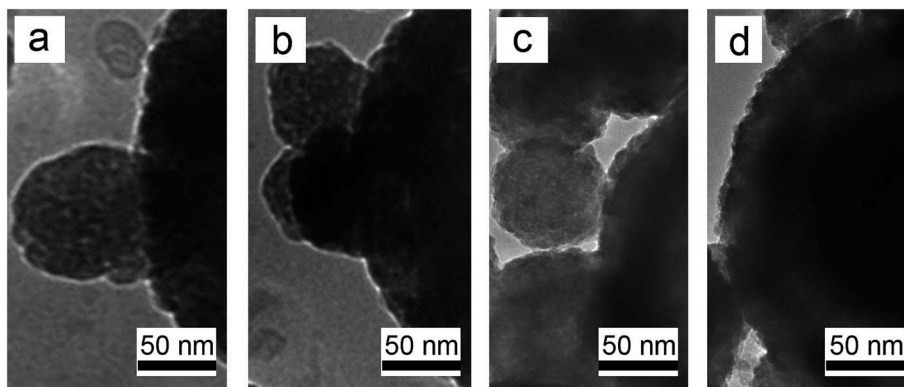


Fig. 5 The TEM image of Ni shell growth process (a–d) for core/shell Fe/Ni MPs.

the diameter of Fe core in our work is approx 300 nm where the Fe core is collected and clustered by a number of Fe NPs, so the value of M_s is close to single-crystalline bulk Fe.⁸ In addition, as a catalytic metal, Ni NP is a ferromagnetic material which M_s is about 40 emu g^{-1} ,^{23,24} like Fe core, the Ni shell is also clustered by a number of Ni NPs. So the M_s of Fe/Ni MP is much higher than that of traditional Fe or Ni NP.^{23,24} Of course, the mechanism underlying the formation of high saturation magnetization is still require more systematic and extensively study.

3.4. Adsorption properties and mechanisms

We put 20 mg of the sample into Cr(vi) concentrations of 20 and 100 mg L^{-1} , respectively (Fig. 8). After 30 minutes, the Cr(vi) ions in the Cr(vi) solutions with concentrations of 10 and 80 mL are adsorbed 71% and 83%, respectively. Due to the high saturation magnetization of the sample, it can be quickly separated from the solution by the external magnetic field after the adsorption equilibrium is reached.

Through the analysis of the HRXPS of adsorbing Cr(vi) on Fe/Ni MPs, three reasons of Cr(vi) reduction debate as following.

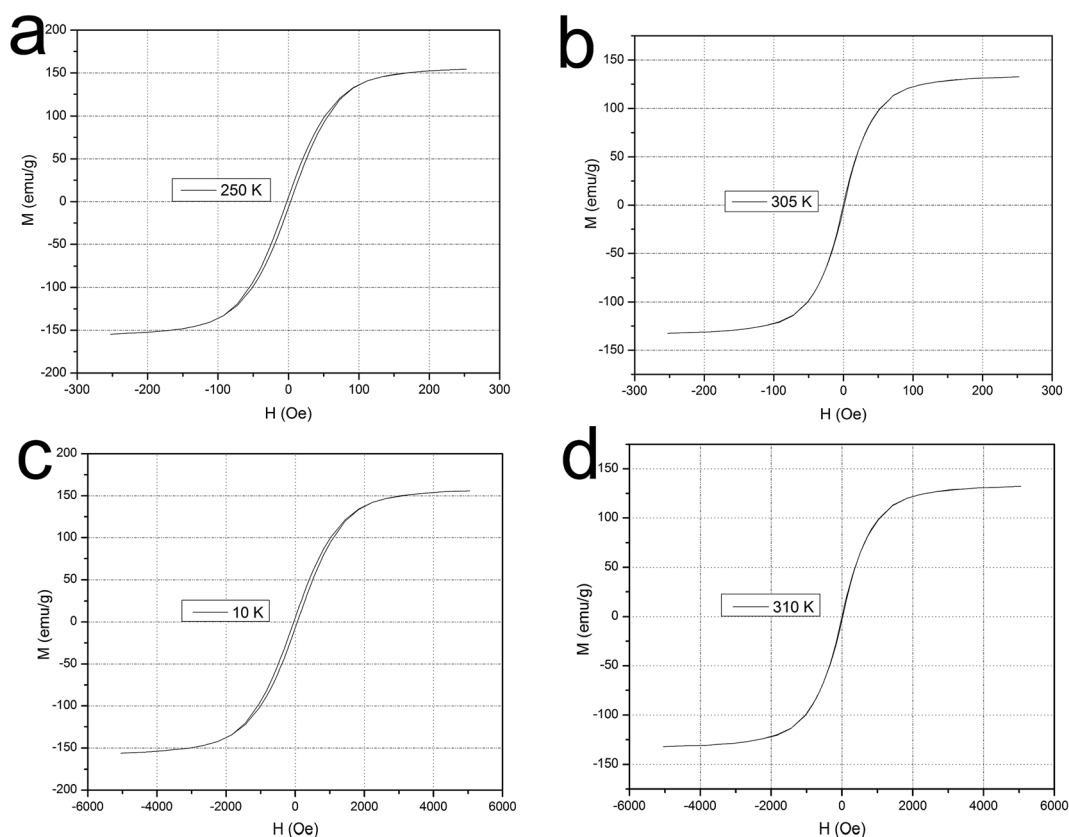


Fig. 6 The magnetization versus curves at 250 K (a) and 305 K (b) in a lower magnetic field (250 Oe), as well as 10 K (c) and 310 K (d) in a higher magnetic field (5000 Oe).



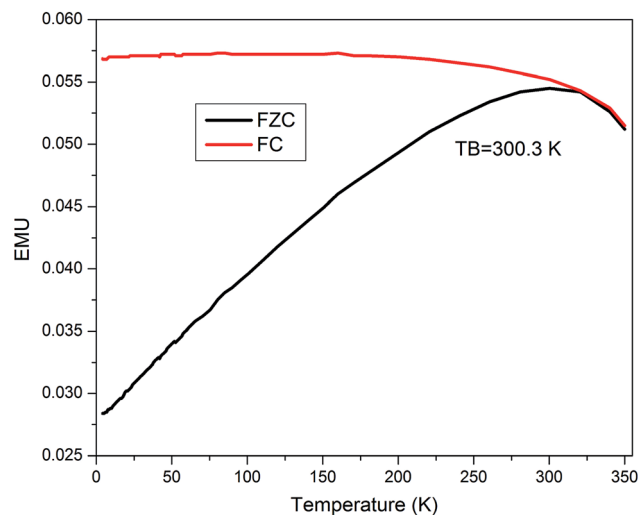


Fig. 7 ZFC and FC curves for the Fe/Ni core/shell MPs.

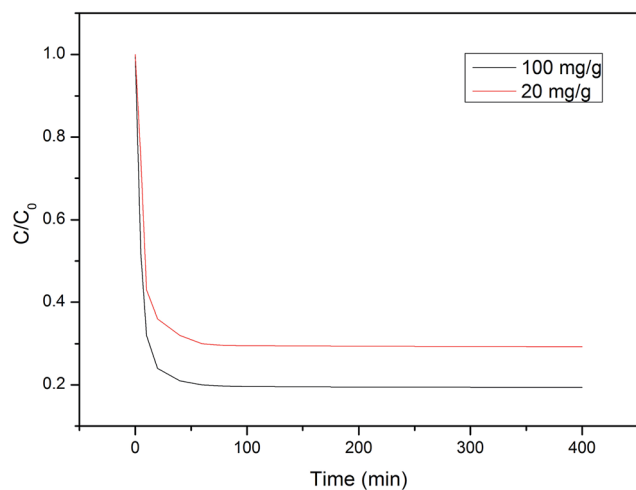
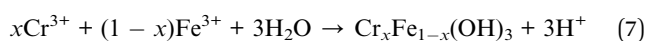
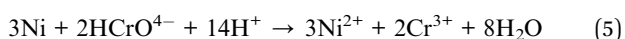
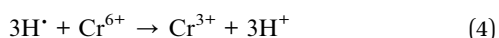
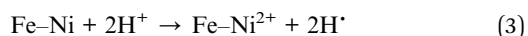


Fig. 8 Effect of time on Cr(VI) removal by MPs.

Firstly, the Cr(VI) is reduced to Cr(III) by reactive H⁺ that catalyzed by Ni. This reaction is expressed by the equations (eqn (3)) and (4). Next, the Fe/Ni bimetallic MPs can form a primary cell, the electrons are transferred from Fe to Ni, and the Cr(VI) is reduced to Cr(III) because the Cr(VI) ions get electrons. A reason for the reduction may be showed in eqn (5) and (6). Finally, due to the high saturation magnetization, the oxyhydroxide co-precipitates formed from the generated Fe(III) and Cr(III) (eqn (7)) could be collected, which is generated on the Fe/Ni MP surface.



4. Conclusions

In this study, the high-quality superparamagnetic core/shell Fe/Ni MPs are successfully synthesized by CVD method and applied to remove Cr(VI) from aqueous solutions. The saturation magnetization of the as-synthesized MPs arrives up to 132.8 emu g⁻¹ at 305 K, which is higher than other ferro-matrix composites. By the analysis of the high-resolution X-ray photoelectron spectrum of the product, the Cr(VI) uptake onto these synthesized magnetite core/shell MPs is identified as a chemical process, including a redox process in which Cr(VI) is reduced into Cr(III), and Cr(III) (may be Cr(OH)₃ and Cr₂O₃) compounds exist on the surface Ni/Fe MPs. Therefore, this study provides an alternative efficient technology to simultaneously reduce and immobilize Cr pollutant.

Conflicts of interest

There are no conflicts of interest to declare.

Acknowledgements

This work is supported by the National Natural Science Foundation of China (21371049, 20971036, and 51372070), Changjiang Scholars and Innovative Research Team in University, No. PCS IRT1126.

References

- 1 V. K. Gupta, S. Agarwal and T. A. Saleh, *Water Res.*, 2011, **45**(6), 2207–2212.
- 2 L. N. Shi, X. Zhang and Z. L. Chen, *Water Res.*, 2011, **45**(2), 886–892.
- 3 J. Zhu, S. Wei, H. Gu, S. B. Rapole, Q. Wang, Z. Luo, N. Haldolaarachchige, D. P. Young and Z. Guo, *Environ. Sci. Technol.*, 2012, **46**(2), 977–985.
- 4 X. Zhou, G. Jing, B. Lv, Z. Zhou and R. Zhu, *Chemosphere*, 2016, **160**, 332–341.
- 5 Y. Wang, B. Zou, T. Gao, X. Wu, S. Lou and S. Zhou, *J. Mater. Chem.*, 2012, **22**(18), 9034–9040.
- 6 Y. Liu, Y. Wang, S. Zhou, S. Lou, L. Yuan, T. Gao, X. Wu, X. Shi and K. Wang, *ACS Appl. Mater. Interfaces*, 2012, **4**(9), 4913–4920.
- 7 S. Xuan, F. Wang, J. M. Lai, K. W. Sham, Y. X. Wang, S. F. Lee, J. C. Yu, C. H. Cheng and K. C. Leung, *ACS Appl. Mater. Interfaces*, 2011, **3**(2), 237–244.
- 8 E. Bian, Y. Xu, S. Lou, Y. Fu and S. Zhou, *J. Nanopart. Res.*, 2016, **18**(11), 331–337.
- 9 T. Liu, Z.-L. Wang, L. Zhao and X. Yang, *Chem. Eng. J.*, 2012, 196–202.
- 10 S. Zhou, Y. Li, J. Chen, Z. Liu, Z. Wang and P. Na, *RSC Adv.*, 2014, **4**(92), 50699–50707.
- 11 X. Weng, S. Lin, Y. Zhong and Z. Chen, *Chem. Eng. J.*, 2013, **229**, 27–34.
- 12 A. Heidari, H. Younesi and Z. Mehraban, *Chem. Eng. J.*, 2009, **153**(1–3), 70–79.



- 13 T. Jaumann, E. M. M. Ibrahim, S. Hampel, D. Maier, A. Leonhardt and B. Büchner, *Chem. Vap. Deposition*, 2013, **19**(7–9), 228–234.
- 14 E. M. M. Ibrahim, S. Hampel, A. U. B. Wolter, M. Kath, A. A. El-Gendy, R. Klingeler, C. Täschner, V. O. Khavrus, T. Gemming, A. Leonhardt and B. Büchner, *J. Phys. Chem. C*, 2012, **116**(42), 22509–22517.
- 15 E. M. M. Ibrahim, S. Hampel, J. Thomas, D. Haase, A. U. B. Wolter, V. O. Khavrus, C. Täschner, A. Leonhardt and B. Büchner, *J. Nanopart. Res.*, 2012, **14**(9), 1118–1126.
- 16 B. Zhao, X. Guo, W. Zhao, J. Deng, G. Shao, B. Fan, Z. Bai and R. Zhang, *ACS Appl. Mater. Interfaces*, 2016, **8**(42), 28917–28925.
- 17 B. S. Kadu, Y. D. Sathe, A. B. Ingle, R. C. Chikate, K. R. Patil and C. V. Rode, *Appl. Catal., B*, 2011, **104**(3–4), 407–414.
- 18 N. Fiol, C. Escudero and I. Villaescusa, *Bioresour. Technol.*, 2008, **99**(11), 5030–5036.
- 19 Y. Y. Zhang, H. Jiang, Y. Zhang and J. F. Xie, *Chem. Eng. J.*, 2013, **229**, 412–419.
- 20 A. D. Bokare, R. C. Chikate, C. V. Rode and K. M. Paknikar, *Appl. Catal., B*, 2008, **79**(3), 270–278.
- 21 H. Yuan, Y. Wang, S.-M. Zhou and S. Lou, *Chem. Eng. J.*, 2011, **175**, 555–560.
- 22 S. Peng, C. Wang, J. Xie and S. Sun, *J. Am. Chem. Soc.*, 2006, **128**(33), 10676–10677.
- 23 E. M. M. Ibrahim, S. Hampel, R. Kamsanipally, J. Thomas, K. Erdmann, S. Fuessel, C. Täschner, V. O. Khavrus, T. Gemming, A. Leonhardt and B. Büchner, *Carbon*, 2013, **63**, 358–366.
- 24 A. A. El-Gendy, E. M. M. Ibrahim, V. O. Khavrus, Y. Krupskaya, S. Hampel, A. Leonhardt, B. Büchner and R. Klingeler, *Carbon*, 2009, **47**(12), 2821–2828.

